

Best Practices for CFD Simulations of Launch Vehicle Ascent with Plumes - OVERFLOW Perspective

Marshall Gusman*, Jeffrey Housman*

ELORET Corporation, 465 S. Mathilda Ave. Suite 103, Sunnyvale, CA 94086

Cetin Kiris†

NASA Ames Research Center, Moffett Field, CA 94035

A simulation protocol has been developed for modeling rocket plumes of heavy lift launch vehicles (HLLV) during ascent. The procedure uses a series of sensitivity studies applied to the Saturn V launch vehicle to establish accurate plume physics modeling of HLLV main engines. These analyses include a comparison of calorically and thermally perfect gas models, a grid dependence study, a sensitivity analysis of nozzle exit boundary conditions for both single and multi-species gas assumptions, and a thorough turbulence model sensitivity study. The results of the analyses are assessed by comparing the predicted plume induced flow separation (PIFS) distance, an important quantity for thermal protection system design. This quantity is also used to validate the results with existing flight data. The viscous Computational Fluid Dynamics (CFD) code OVERFLOW, a Reynolds Averaged Navier-Stokes flow solver for structured overset grids is utilized. This work is a continuation of the CFD best practices for Ares V aero-database simulation,¹ with the additional complexity of plume physics modeling.

Nomenclature

D	: Reference diameter, m
Re_D	: Reynolds number based on D
M_∞	: Free-stream Mach number
P_∞	: Free-stream pressure, Pa
T_∞	: Free-stream temperature, °K
ρ	: Density, kg/m ³
c	: Speed of sound, m/s
T	: Temperature, °K
y^+	: Non-dimensional wall spacing
PIFS	: Plume-induced flow separation
SA	: Spalart Allmaras 1-equation turbulence model
SST	: Shear-Stress Transport 2-Equation Turbulence model
SST-00	: SST turbulence model with no corrections
SST-10	: SST turbulence model with curvature correction
SST-01	: SST turbulence model with temperature correction
SST-11	: SST turbulence model with curvature and temperature correction

*Aerospace Engineer

†Branch Chief

I. Introduction

High-fidelity modeling and simulation is currently being used in NASA's development of next generation launch vehicles, including a Heavy Lift Launch Vehicle (HLLV) for carrying large payloads to low earth orbit. The best practice protocol provides information on the necessary mesh resolution requirements, physical models, boundary conditions, and turbulence models to accurately predict the quantities of interest. In the context of HLLV ascent, some of the quantities of interest include aerodynamic force and moment coefficients and load distributions, as well as base heating and surface pressure estimates. To provide acceptable predictions of these quantities, the CFD simulations must accurately model the physics of the exhaust plume as it expands with increasing altitude. The purpose of this study is to investigate the CFD requirements to accomplish this goal, as a first step in developing current CFD practices for plumes. This work, along with work in USM3D,² is a continuation of the CFD best practices for aero-database generation of Ares V during ascent, Kiris et al.¹

Rockets at high-altitude are subject to a fluid dynamics phenomenon known as Plume-Induced Flow Separation³ (PIFS). Flow separation occurs when an adverse pressure gradient forces the boundary layer to detach from the surface of the rocket. One cause of the adverse pressure gradient during ascent is the expansion of the exhaust plume as the rocket gains altitude. In a low ambient pressure environment, the high pressure at the nozzle exit rapidly expands the exhaust jet in both downstream and radial directions. This produces an obstruction to the free-stream flow which forms an adverse pressure gradient near the aft section of the rocket. Ultimately, the flow separates and recirculation from the base of the vehicle to the upstream separation point allows convective transport of hot exhaust gas along the surface of the vehicle. The distance between the end of the vehicle and the separation point of the surface is denoted as the PIFS distance. Accurate prediction of the PIFS distance is critical to the design of the thermal protection system, and will be used in this study to quantify the accuracy of the computed results. The purpose of this work is to demonstrate, through a series of sensitivity studies, the modeling and simulation requirements for accurate plume physics modeling and PIFS distance prediction of HLLVs during ascent. The Saturn V launch vehicle is used in this study as a representative HLLV, and flight data from the launch of Apollo 11 is used to validate the computed results.

In this paper, a preliminary study is performed to compare plume modeling for two multi-species gas models. This two-dimensional axisymmetric jet expansion problem was performed with the commercial CFD software, Star-CCM+,⁴ to evaluate the calorically perfect gas assumption used in the NASA-developed CFD code OVERFLOW.⁵ OVERFLOW is a viscous Reynolds Averaged Navier-Stokes (RANS) flow solver for high Reynolds number turbulent flows using structured overset grids. OVERFLOW is used to perform all three-dimensional plume simulations reported in this paper. A series of sensitivity and validation studies are performed to determine the best practices for plume simulations and predictions of PIFS. These studies include a near-wall grid resolution study, sensitivity analysis of nozzle exit boundary conditions for multi-species flow models, a comparison between the multi-species gas model and single species gas model assumptions, and a detailed turbulence modeling sensitivity study. Best practices resulting from these studies are summarized in the conclusion.

The current work builds on the knowledge and experience attained through previous studies on other launch vehicles. These studies include work on the Space Shuttle,⁶ best practices for overset grid generation,⁷ best practices for Orion,⁸ and best practices for ascent aerodynamics of Ares I.⁹

II. Problem Description

Simulations in this paper are performed using the Saturn V launch vehicle during ascent, with the inclusion of exhaust plume effects. Saturn V is an Apollo-era launch vehicle, with a vertical-stack design that resembles design concepts for future heavy lift launch vehicles currently being developed at NASA. Data for the Saturn V's trajectory, geometry, and flight performance is publicly available, along with flight data such as PIFS distance. All flight trajectory information is derived from the Flight Evaluation report from the launch of Apollo 11.¹⁰

The vehicle is 110.7 meters tall with five F-1 liquid rocket engines each generating approximately 8×10^6 Newtons of thrust to propel the rocket through its ascent trajectory. In video recordings of the flight, plume-induced flow separation is observed for Mach numbers greater than approximately 3.3, as shown in a frame from one of the videos in Figure 1(a). The hot exhaust gas radiates orange and yellow and reveals

the extent of plume induced flow separation up the sides of the vehicle. PIFS distance measurements were made from video footage of the launch, and contain an uncertainty of approximately 10%. At Mach 4.4, PIFS was measured at 15 meters from the vehicle reference station 0, see Figure 1(b) for a diagram of PIFS measurements. To reduce loads on the vehicle and crew, the center engine cut-off (CECO) event occurs at 136 seconds, leading to a brief reduction in PIFS distance before it climbs back to 33 meters at Mach 6.5. Steady-state simulations were performed at four points in the ascent trajectory with corresponding supersonic Mach numbers 1.5, 2.7, 4.4, and 6.5. A description of the flow solvers used in this study is presented in the next section.

Table 1. Free-stream conditions for Saturn V PIFS simulations.

M_∞	P_∞ (Pa)	T_∞ (°K)	Re_D
1.5	12111.0	217	6.1522×10^7
2.7	2250.0	221	2.2623×10^7
4.4	151.0	264	1.6970×10^6
6.5	22.0	247	4.0600×10^5

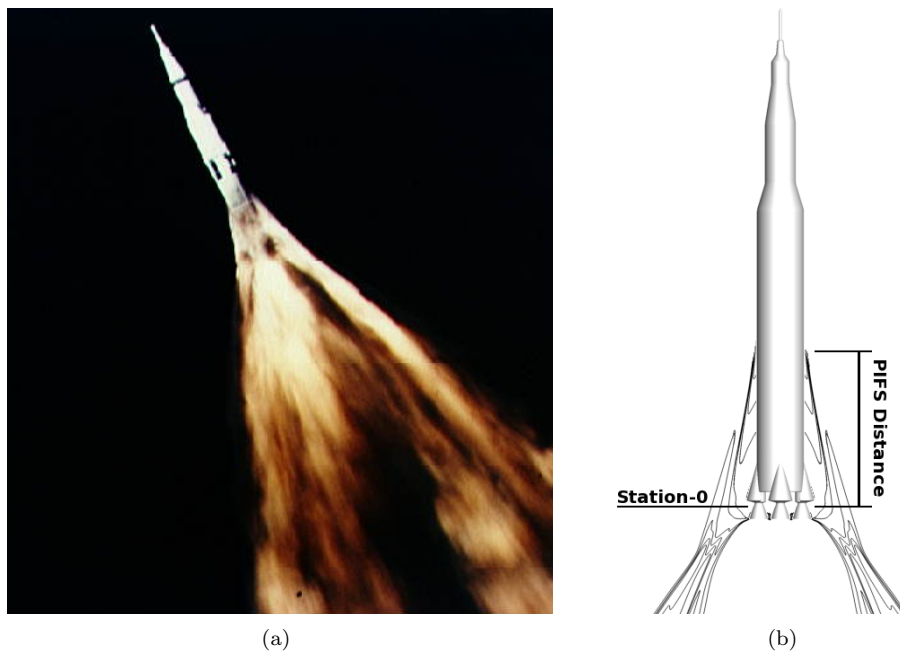


Figure 1. PIFS examples: (a) frame from chase plane footage of Apollo 6 flight with PIFS visible by extent of radiating exhaust gas, and (b) diagram of Saturn V station zero (located 2.8 m from the nozzle exit) and measurement of PIFS distance.

III. CFD Solvers

A. OVERFLOW

The NASA flow solver OVERFLOW-2 is used to simulate the viscous flow field around the Saturn V launch vehicle with exhaust plumes. OVERFLOW is an implicit structured overset Reynolds-Averaged Navier-Stokes (RANS) solver for structured overset grids. Second-order central-differencing with explicit artificial dissipation is used for the convective fluxes. The Beam-Warming block tri-diagonal implicit ADI scheme is run in parallel using domain decomposition and the Message Passing Interface (MPI) standard. The solver was run on the Columbia and Pleiades supercomputers at NASA Ames Research Center, using 128 processors

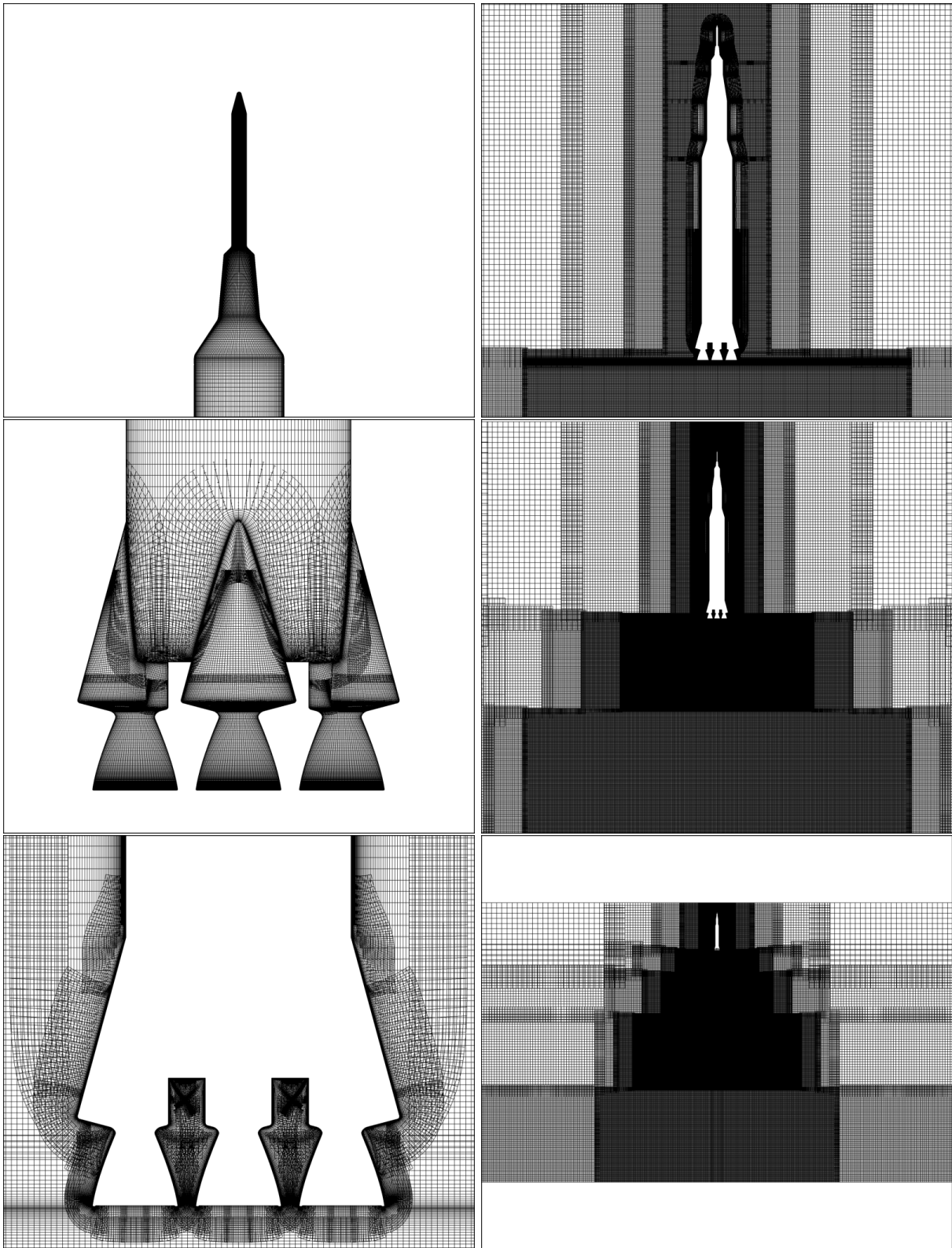


Figure 2. Surfaces and slices of the overset grid system for the Saturn V.

and approximately 36 hours of runtime for each steady state run. Structured viscous overset grid systems were built to represent the geometry of the Saturn V flight vehicle using grid generation scripts based on the Chimera Grid Tools (CGT) script library.¹¹ The overset grid system for Saturn V, see Figure 2, contains 67 zones and approximately 52-60 million grid points. A hierarchy of successively refined cylindrical off-body grids are used to discretize the external domain. The off-body grids shown on the right of Figure 2 were created in the plume region to maintain high resolution for all points in the trajectory. Using cylindrical grids allows the plume to remain well-resolved in the off-body using fewer mesh points than a Cartesian off-body grid system. Typical convergence results are shown in Figure 3, where the residual convergence is plotted on the left and the force convergence is plotted on the right. The large spikes in the early stages of the residual plot are caused by a successive reduction of the artificial dissipation parameters from relatively large values to the default values described in the OVERFLOW manual, see Ref. 5. Modifying the dissipation parameters during the development of the steady solution allows the use of a large CFL number throughout the computations, and leads to overall faster convergence of the problem. The nozzle exit boundary conditions used for the simulations are described in detail in Section V.

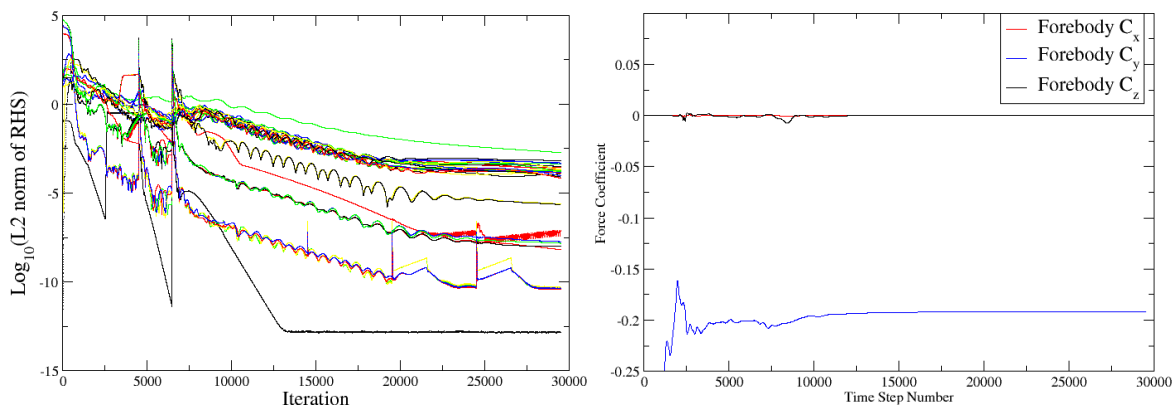


Figure 3. Convergence history of the OVERFLOW residuals (left) and forces (right) for the Saturn V.

B. Star-CCM+

The commercial software package Star-CCM+ is used to compare the calorically perfect gas assumption with the thermally perfect gas model for simulations of plume expansion. Star-CCM+ is an unstructured polyhedral finite-volume Navier-Stokes flow solver. The code is made parallel using domain decomposition and MPI message passing. The inviscid fluxes are discretized using Roe flux difference splitting¹² with MUSCL extrapolation and central-differencing for the viscous fluxes. An implicit point Gauss-Seidel procedure is used to iterate to steady-state along with algebraic multigrid for convergence acceleration.

IV. Plume Physics

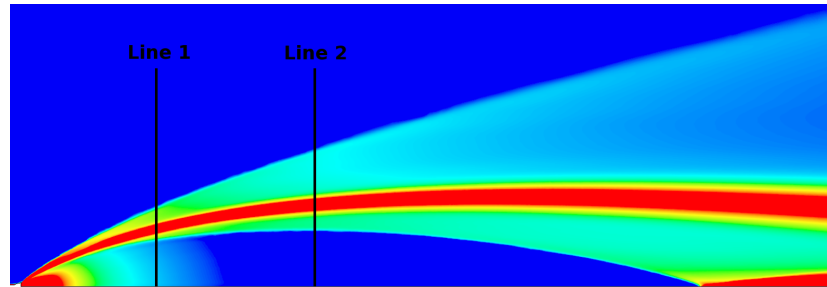
The exhaust plume emitted from a liquid rocket engine is a complex flow field composed of a chemically reacting mixture of gases and unburned liquid fuel. In Table 2, five categories of plume physics modeling are described in descending levels of complexity. Each model is listed with its requirements, limitations, and examples of available CFD software that have implementations of the model. The best practices for CFD support of HLLV design requires accurate predictions of flow phenomena such as PIFS distance. For efficient use of computational resources, the least expensive model which predicts the relevant quantities of interest should be used. The two most commonly implemented and tested choices are the single-species perfect gas model and the calorically perfect multi-species model, both of which are available in OVERFLOW. To determine the differences between the calorically perfect and thermally perfect multi-species gas assumptions on modeling plume expansion, Star-CCM+ was applied to a two-dimensional axisymmetric nozzle case using these two different gas models.

Table 2. Plume physics modeling hierarchy

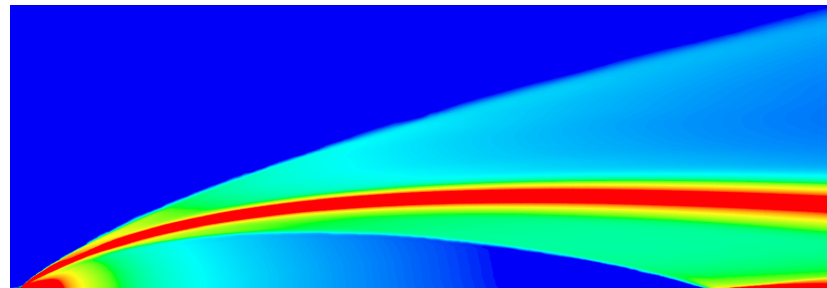
Model	Requirements	Excludes	Examples
Multi-Phase Reacting Flow	Complex equation of state (EoS), detailed finite-rate chemistry (hard to find), multi-phase closure, large computational expense	–	Research codes, some commercial codes with limited success
Multi-Species Reacting Flow	Complex EoS, detailed finite-rate chemistry, significant computational expense	Liquid and solid phases	Loci-CHEM, DPLR, LAURA, commercial codes
Multi-Species Thermally Perfect Gas	Complex EoS for each species, $c_p(T)$ and $c_v(T)$	All of the above, finite-rate chemistry	Loci-CHEM, DPLR, LAURA, commercial codes
Multi-Species Calorically Perfect Gas	EoS for each species, c_p and c_v , reasonable simulation time	All of the above, temperature effects	OVERFLOW, Loci-CHEM, commercial codes
Single Perfect Gas	EoS	All of the above, multi-species gas physics	OVERFLOW, USM3D, Cart3D

A. Comparison of Multi-Species Gas Models

A generic axisymmetric rocket engine was studied to understand the effects of multi-species gas models on plume expansion. Correct plume expansion is critical for PIFS predictions. The axisymmetric test case is intended to verify that plume expansion of a calorically perfect gas coincides with that of a thermally perfect gas. A thermally perfect gas has temperature-dependent specific heat coefficients, while a calorically perfect gas assumes constant specific heat coefficients. The gas models are compared using the commercial software Star-CCM+ on a two-dimensional axisymmetric polyhedral mesh with user-specified refinements for the plume region.



(a) Thermally perfect gas



(b) Calorically perfect gas

Figure 4. Steady-state temperature contours for axisymmetric nozzle with two gas models.

For the thermally perfect multi-species model, Marshall Space Flight Center (MSFC) engineers provided the temperature-dependent specific heat coefficients of exhaust gas.¹³ Supersonic free-stream flow conditions are imposed upstream and external to the nozzle. The RANS equations are solved to steady-state with three to four orders of magnitude reduction in the residual using the $k-\omega$ SST turbulence model. The steady-

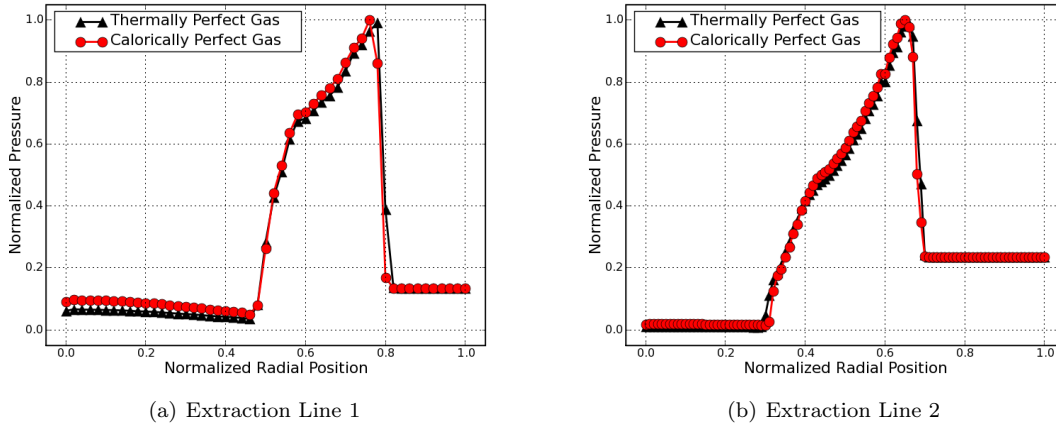


Figure 5. Comparison of pressure from three gas models along extraction lines from Figure 4(a).

state temperature contours in Figure 4 show that plume expansion is indistinguishable between the two multi-species gas models. Compared to the thermally perfect gas, the calorically perfect gas over-predicts temperatures in the plume core and slightly under-predicts temperatures in the mixing layer.

Differences in plume expansion are shown using line plots of pressure extracted from radial lines at two downstream locations, shown in Figure 5. Each line corresponds to a cross-section of the plume, as shown in the overlay of Figure 4(a). Peak pressure magnitude and shock locations are nearly identical for the multi-species gas models, and no significant differences are observed in the predicted plume expansion. Since the plume expansion is the dominating physics in computing the PIFS distance, the calorically perfect gas is a suitable model.

V. Sensitivity and Validation Studies with Saturn V

The plume physics modeling study is extended to the full-scale three-dimensional Saturn V launch vehicle. To assess the accuracy of the CFD approach for predictions of plume induced flow separation, a sensitivity and validation study is performed. A grid dependence study is conducted to determine the effects of wall spacing on PIFS prediction. Next, different nozzle exit boundary conditions are analyzed to determine their effect on PIFS distance. A final study of the PIFS distance sensitivity to the turbulence model was conducted using the Spalart-Allmaras¹⁴ and Shear Stress Transport¹⁵ turbulence models. Validation with existing flight data was considered throughout the studies. Results of this work were used to establish best practices for HLLV ascent simulations including plumes.

A. Viscous Wall Spacing Study

To eliminate grid dependence, a viscous wall spacing study is performed. Off-body grid resolutions are consistent with previous work, as presented in the companion paper.¹ In general, a non-dimensional wall spacing $y^+ \approx 1.0$ is considered sufficiently refined to capture the momentum boundary layer and provide accurate flow solutions. However, flow separation and temperature effects may change the solution's sensitivity to wall spacing. To quantify the effects of wall spacing, the Saturn V launch vehicle is simulated at Mach 6.5 using OVERFLOW's multi-species gas model on four different near-body grid systems. The near-body grid systems were originally created to provide $y^+ = 0.9$ wall spacings for four conditions in the Saturn V flight trajectory from Mach 1.5 to 6.5. These grids have a dimensional wall spacing that ranges from 5.0×10^{-6} to 5.0×10^{-4} meters, which when used at the Mach 6.5 flight conditions, provide dimensionless y^+ wall spacings ranging from 0.01 to 0.9. Figure 6 compares PIFS distances on each grid using both the SA and SST turbulence models. The predicted PIFS distance changes less than 3% for the SST model and 6% for the SA model across the grids used in the study. PIFS distance variations of this size indicate that sufficient grid resolution is achieved even at the largest wall spacing. Differences between PIFS predictions using the two turbulence models will be addressed in the section on turbulence modeling.

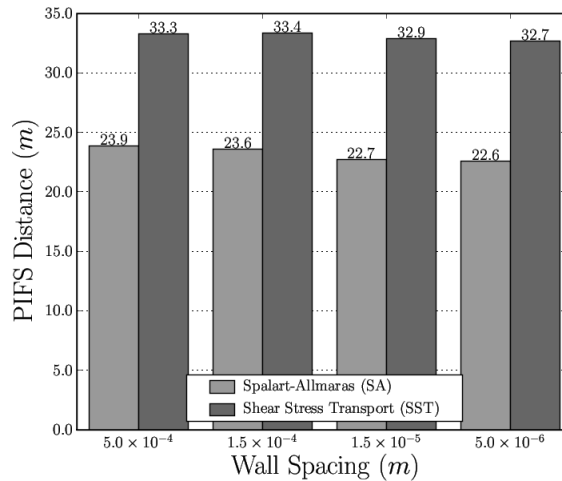


Figure 6. Effect of wall spacing on predicted PIFS distance for Saturn V at Mach 6.5, SST model with no corrections.

B. Nozzle Boundary Condition Approaches for Plumes

Plume simulations often depend on limited information about the nozzle exit conditions. When only the mean exit conditions are provided, the quasi one-dimensional isentropic nozzle relations can be used to compute stagnation conditions at the nozzle plenum (chamber). The nozzle interior geometry is required as input for the nozzle relations and must be included in the three-dimensional computational grid. This may increase the number of grid points by up to 15%, depending on the number of engines. Another method is to apply boundary conditions at the nozzle’s exit plane. The simplest option is to apply the mean exit conditions uniformly across the nozzle exit, but this is a crude approximation to the actual exit conditions and predicts inaccurate plume expansion. Preferably, radially-varying exit conditions should be provided, but in most cases a CFD solver must be used to obtain the exit conditions. One option used in the present study is a multi-phase reacting flow solver for two-dimensional axisymmetric nozzles.¹⁶ This code models fuel combustion, solid particle interactions, and multi-phase flow effects. The final option evaluated in this study uses OVERFLOW to simulate a two-dimensional axisymmetric nozzle and provide nozzle exit conditions for the full three-dimensional simulation. Both the high-fidelity and OVERFLOW BC options exhibit radially varying profiles with higher lip pressures and lower center line pressures than the uniform conditions. No radial component of velocity nor axial velocity boundary layer is provided for the uniform conditions.

PIFS predictions for the Saturn V are compared using three nozzle exit boundary condition options. These options include uniform exit conditions, OVERFLOW-derived exit conditions, and conditions provided by the high-fidelity multi-phase solver. OVERFLOW’s calorically perfect multi-species gas model is used to simulate the vehicle at Mach 6.5 with four F-1 engines firing. Figure 7 shows streamlines and axial velocity contours for each nozzle boundary condition applied. The extent of PIFS is indicated by the blue contour extracted from one grid point above the surface (approx. 0.5 millimeters). Similar PIFS distances are predicted using the high-fidelity BC and the OVERFLOW BC, while applying uniform mean exit conditions generates lower PIFS distance. This is caused by the smaller plume expansion in the uniform BC simulation, which lacks a radial component of velocity and has much lower lip pressure than the other boundary condition options. Figure 8(a) contains a plot of the axial velocity 0.5mm above the surface of the vehicle, showing the extent of flow separation in the regions of positive velocity. This corresponds to the dark blue velocity contours in Figure 7, and the predicted PIFS distances in the bar chart of Figure 8(b). The predicted PIFS distance is within 1% of the flight data when using the high-fidelity boundary condition. The OVERFLOW boundary condition over-predicts by 7.5%, and the uniform boundary condition under-predicts by 53%. Note that the 11% uncertainty in the flight data makes the differences between the two radially-varying boundary conditions less significant. This study has also indicated that PIFS is sensitive to the nozzle exit boundary condition.

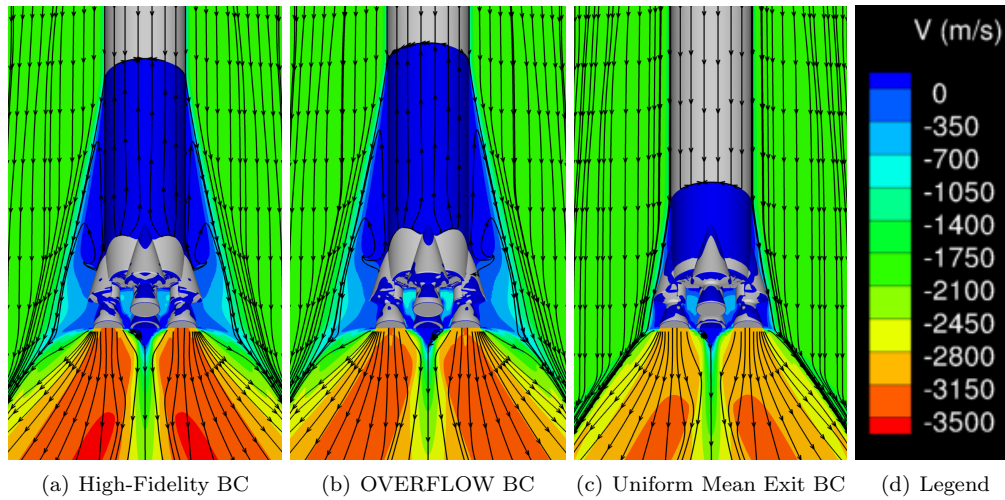


Figure 7. Streamlines and steady state axial velocity contours showing PIFS for three types of boundary conditions. Dark blue regions designate the extent of reversed flow.

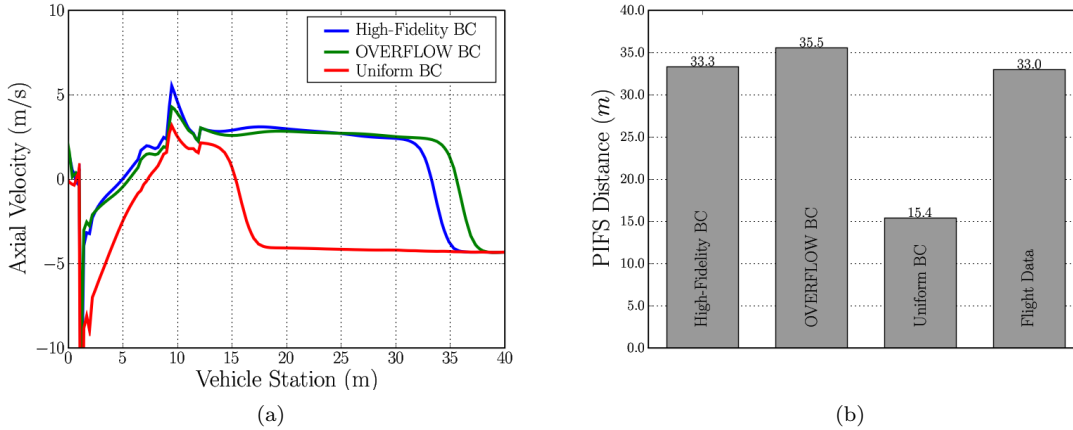


Figure 8. Effect of nozzle exit boundary conditions on predicted PIFS distance for Saturn V at Mach 6.5. (a) Axial velocity 0.5mm above the body, from station zero to 40 meters, (b) computed PIFS distance.

C. Accuracy of Single-Species Gas Model

Single species simulations are more computationally affordable than multi-species, and require less information about the exhaust gas properties. However, proper specification of nozzle exit boundary conditions is necessary to predict the correct plume behavior. The multi-species model uses a different equation of state for each gas, allowing all nozzle exit conditions to be matched. Alternatively, the single-species model uses one equation of state, which only allows two out of three thermodynamic quantities to be matched. For the present results, an ideal gas equation of state with $\gamma = 1.4$ is used for the single-species gas model. By matching the pressure (p) and three components of velocity (u, v, w) at the exit, the system only allows one more quantity to be specified. The choices are to maintain density (ρ), temperature (T), or sound speed (c). The problem is that by preserving any one of these conditions, the other two will differ from the true multi-species nozzle exit conditions. OVERFLOW simulations using these three thermodynamic closure options are compared to determine which option best matches the multi-species results.

The radially-varying exit conditions for an F-1 engine are compared in Figure 9. The high-fidelity data is closely matched by the $\gamma = 1.24$ boundary conditions for a multi-species simulation. Three $\gamma = 1.4$ boundary

conditions for single-species OVERFLOW simulations are shown, which preserve pressure and velocity, and either density, sound speed, or temperature. The $\gamma = 1.4$ assumption causes the fluid relations to differ from the actual exhaust gas, so matching temperature causes incorrect Mach and density, matching sound speed gives the correct Mach number but incorrect temperature and density, and matching density causes incorrect temperature and Mach number.

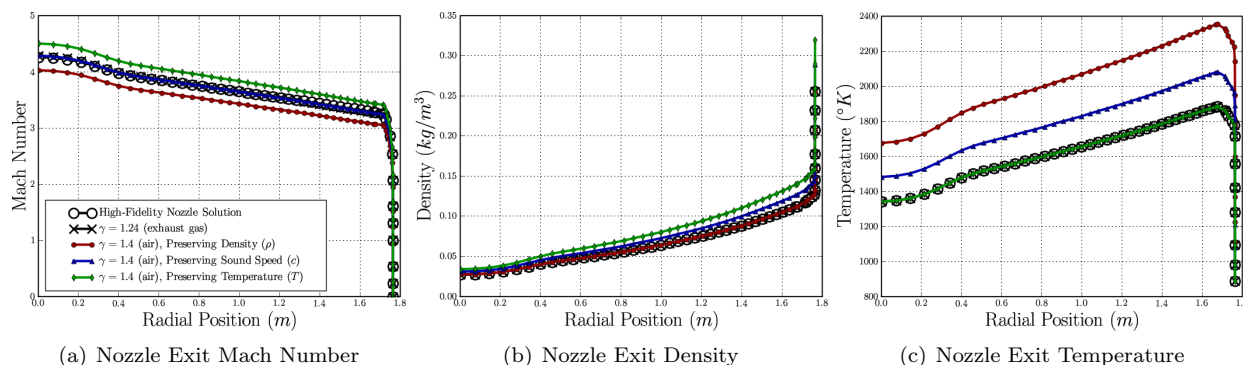


Figure 9. Radially-varying nozzle exit profiles comparing the single-species and multi-species assumptions with high-fidelity boundary conditions for Saturn V F-1 engines.

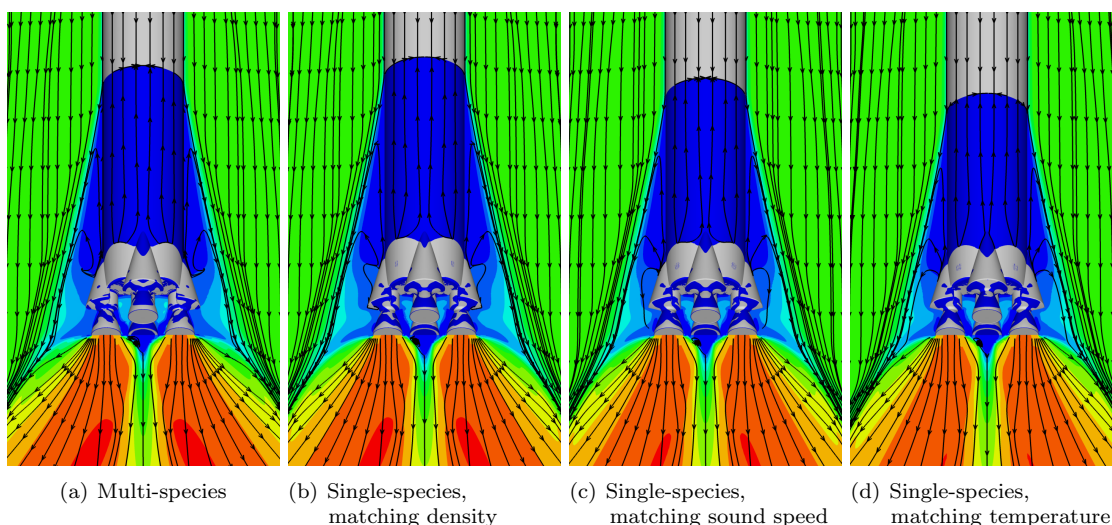


Figure 10. Streamlines and steady state axial velocity contours showing PIFS for multi- and single-species boundary conditions. Blue regions designate the extent of reversed flow.

Figure 10 shows axial velocity contours near the surface and on a slice through the flow field, while Figure 11(a) contains a plot of the axial velocity 0.5mm above the surface of the vehicle. Each boundary condition creates a slightly different plume expansion downstream of the vehicle, and the angle of the plume expansion determines the extent of the reversed flow from the vehicle's base to the PIFS location. Predicted PIFS distances for each of three single-species plume simulations are shown in Figure 11(b). The best match to the multi-species solution is achieved when density is preserved at the exit, with a predicted PIFS distance within 4%. By preserving density at the nozzle exit, thrust and mass flow rate are consistent with the $\gamma = 1.24$ boundary condition. When Mach number is preserved the PIFS distance is 6% less, and when temperature is preserved the PIFS distance is 13% less than the multi-species solution. Further investigation is needed to validate the single-gas assumption for heating effects and pressure signatures on the base.

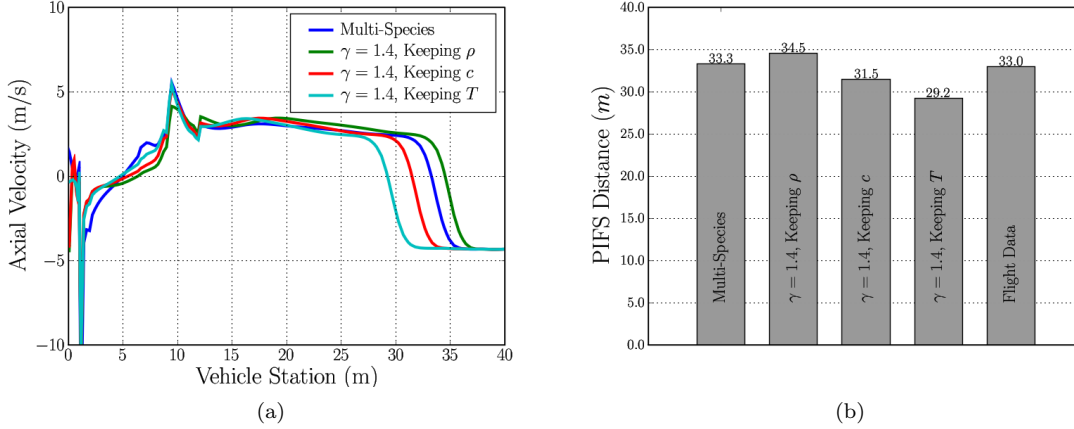


Figure 11. Effect of single-species boundary condition implementations on predicted PIFS distance for Saturn V, compared against multi-species and flight data. (a) Axial velocity 0.5mm above the body, from station zero to 40 meters, (b) computed PIFS distance.

D. Turbulence Modeling

PIFS is directly related to many viscous flow features, which in turn depend on turbulence modeling. Flow features such as boundary layer growth, flow separation, plume shear layers, and turbulent mixing are highly sensitive to viscosity. To determine the appropriate turbulence model for PIFS simulations, an investigation of turbulence model effects is conducted.

Using the established grid resolution and nozzle exit boundary conditions, calorically perfect multi-species calculations were conducted with the SA and SST (no corrections) turbulence models at Mach numbers 1.5, 2.7, 4.4, and 6.5. These results will be used to assess the turbulence models' effect on PIFS distance and to compare with flight data. Except for Mach 6.5 which occurs after CECO, all five engines are firing. This difference can be seen in Figure 12, where Mach contours on a slice through the domain are plotted for each simulation. As the free-stream Mach number rises, the angle of the bow shock decreases and the expansion angle of the plume increases. Capturing the correct plume expansion angle is critical for predicting the correct PIFS distance. As the vehicle gains altitude, the ambient pressure decreases while the nozzle exit pressure remains constant. This creates a high pressure ratio between the nozzle exit and the ambient air, which causes the plume to expand radially. This creates a large obstruction to the incoming flow and generates plume-induced flow separation. Evidence of the increasing PIFS distance with Mach number is shown in Figure 12, where the PIFS regions are identified by the lowest Mach contour levels shown in blue.

Predicted PIFS distances for the two turbulence models are compared to flight data from the AS-506 launch of Apollo 11 in Figure 13(a). The lowest two Mach numbers exhibit no PIFS except for recirculation in the base region of the vehicle. From Ref. 10, station zero corresponds to a point mid-nozzle, so the minimum PIFS is plotted at 2.8 meters, the distance from station zero to the base of the vehicle. At Mach 4.4, CFD-predicted flow separation for the SA model has travelled up the vehicle to a distance of 10.8 meters, while the SST predicts 16.1 meters. The SST model is more consistent with the observed flight data of 15 meters. At Mach 6.5 and after CECO, the predicted PIFS distance using the SST model is once again more consistent with flight data, with a distance of 33.3 meters compared to 33.0 meters. The SA model under-predicts the observed flight data, showing only 23.9 meters of PIFS distance.

At Mach 6.5 where the maximum PIFS distance occurs, an additional turbulence model study is performed to assess the different combinations of curvature and temperature correction terms available in the SST implementation in OVERFLOW. The curvature correction is intended to reduce excessive eddy viscosity generated by the turbulence model in rotating and curved flow regions,¹⁷ while the temperature correction term should balance the effect of large temperature gradients present in exhaust plume simulations.¹⁸ Four permutations of these correction terms were compared using the SST model; no corrections (SST-00), curvature correction (SST-10), temperature correction (SST-01), and both curvature and temperature corrections (SST-11). Figure 13(b) displays the results of this comparison. Including the SST corrections for curvature

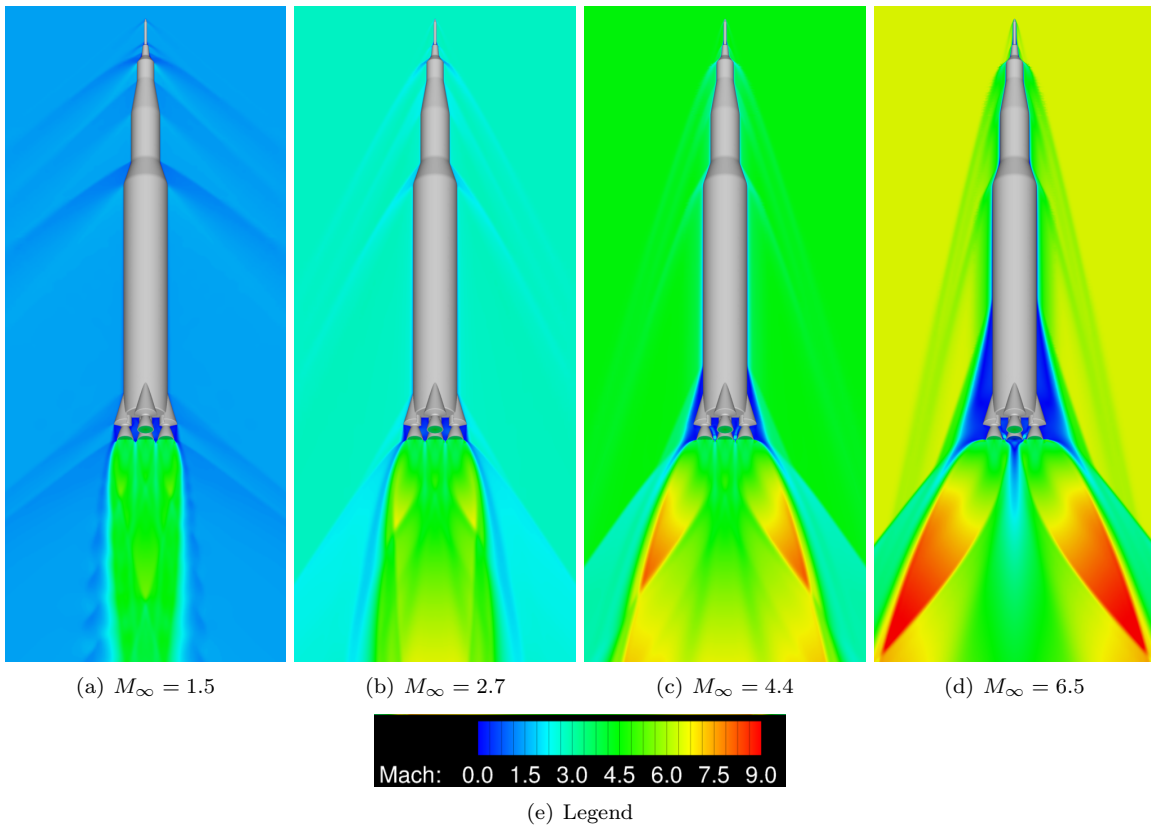


Figure 12. Mach contours at four points in the Saturn V's ascent trajectory, using the SST turbulence model without corrections.

or temperature decreases the PIFS distance by approximately 3 and 6 meters, respectively. Using both corrections (SST-11) accumulates the effect with a total decrease of 8 meters, and yields a PIFS distance within 6% of the SA model's result. The correction terms applied to the SST model exhibit negative effects on PIFS distance prediction.

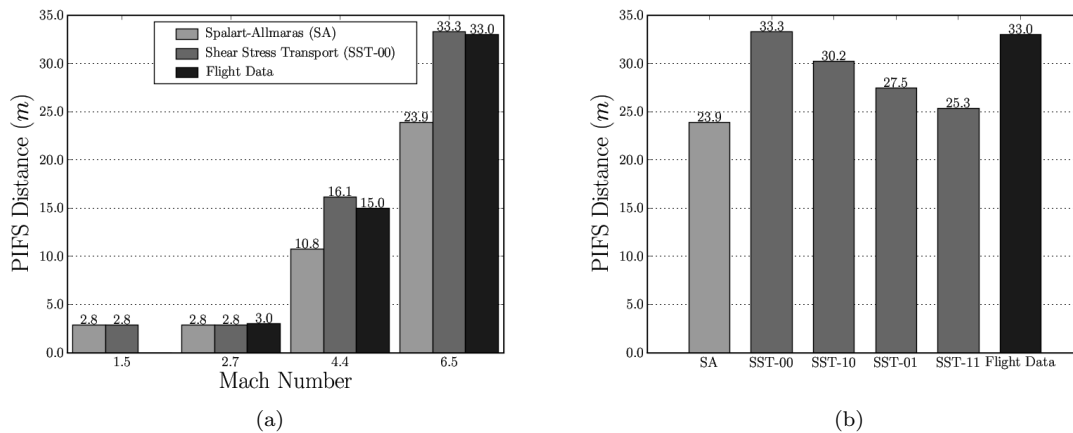


Figure 13. PIFS distances for SA and SST turbulence models with flight data. (a) compared across selected trajectory points, and (b) Mach 6.5 conditions examining curvature and temperature correction variations.

The differences observed between the SA and SST models can be explained by an examination of the

plume expansion and shear layer. Figure 14 shows velocity vectors colored by magnitude near the lower aft section of an outer nozzle (see Figure 15(c) for a diagram of this location on the vehicle). The velocity vectors show a more diffused plume shear layer in the solution using the SA model, as indicated in the circled region. The excessive diffusion is due to a higher and more diffused turbulent eddy viscosity (μ_T) field in the SA solution in comparison to the SST-00 solution. Contour plots of the normalized μ_T for SA and SST-00 models are shown in Figure 15(a) and (b). The additional μ_T diffuses the plume expansion and leads to the lower PIFS distance prediction for the SA model. Including correction terms in the SST model changes the production of μ_T , as seen in Figure 15(d)-(f). The curvature correction reduces the maximum μ_T , but diffuses it across the shear layer, which leads to a slightly reduced plume expansion angle. The temperature correction generates significantly higher μ_T in the shear layer, resulting in a noticeably reduced expansion angle. Combining the two corrections leads to the highest and most diffused μ_T field, and results in a plume expansion angle and PIFS distance similar to the SA model.

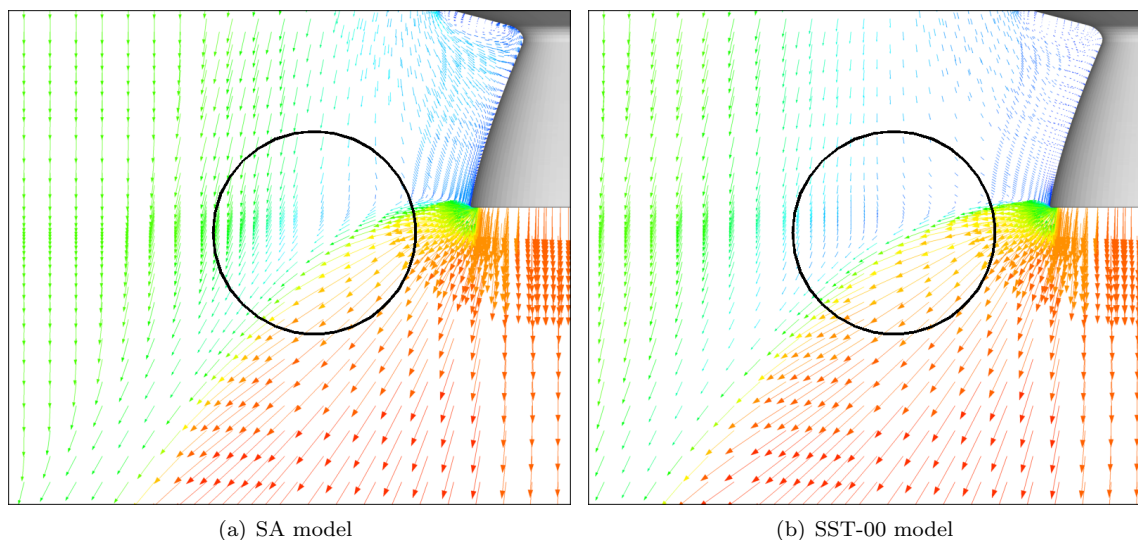


Figure 14. Velocity vectors colored by magnitude on a slice through an outer F-1 nozzle. Plume shear layer region of interest circled in black

Using the lessons learned from the sensitivity studies, CFD predictions for Mach numbers 2.7, 4.4, and 6.5 using the SST turbulence model (SST-00) are overlaid at appropriate locations in Figure 16. At Mach 4.4, CFD-predicted flow separation has crept up the vehicle to a distance of 16 meters, comfortably within the scattered flight data at this trajectory point. After CECO, the predicted PIFS distance at Mach 6.5 is 33.3 meters, which is directly on top of the flight data.

VI. Conclusions

A computational approach for plume simulations of HLLV ascent has been developed. Best practices for these simulations were assessed based on predictions of plume-induced flow separation on the Saturn V at high altitude and Mach conditions. Initially, a CFD code was used to verify that the calorically perfect gas assumption predicts similar plume expansion to the thermally perfect model for an axisymmetric plume. A sensitivity and validation procedure was performed using the OVERFLOW CFD code for simulations of the Saturn V launch vehicle including plumes at four points in the ascent trajectory. This work included a near-wall grid resolution study, a plume boundary condition study for single and multi-species gas models, and a turbulence model study. Flight data was used to validate these results, which have been used to define CFD best practices for simulating HLLV ascent with plumes.

Results from the near-wall grid spacing study demonstrated that a $y^+ = 0.9$ provided sufficient resolution for predicting PIFS distance, with variations less than 3 to 6%. The best comparisons with flight data were provided by a boundary condition from a high-fidelity rocket nozzle code. An examination of single-species boundary conditions showed that by matching pressure, velocity, and density at the nozzle exit, good

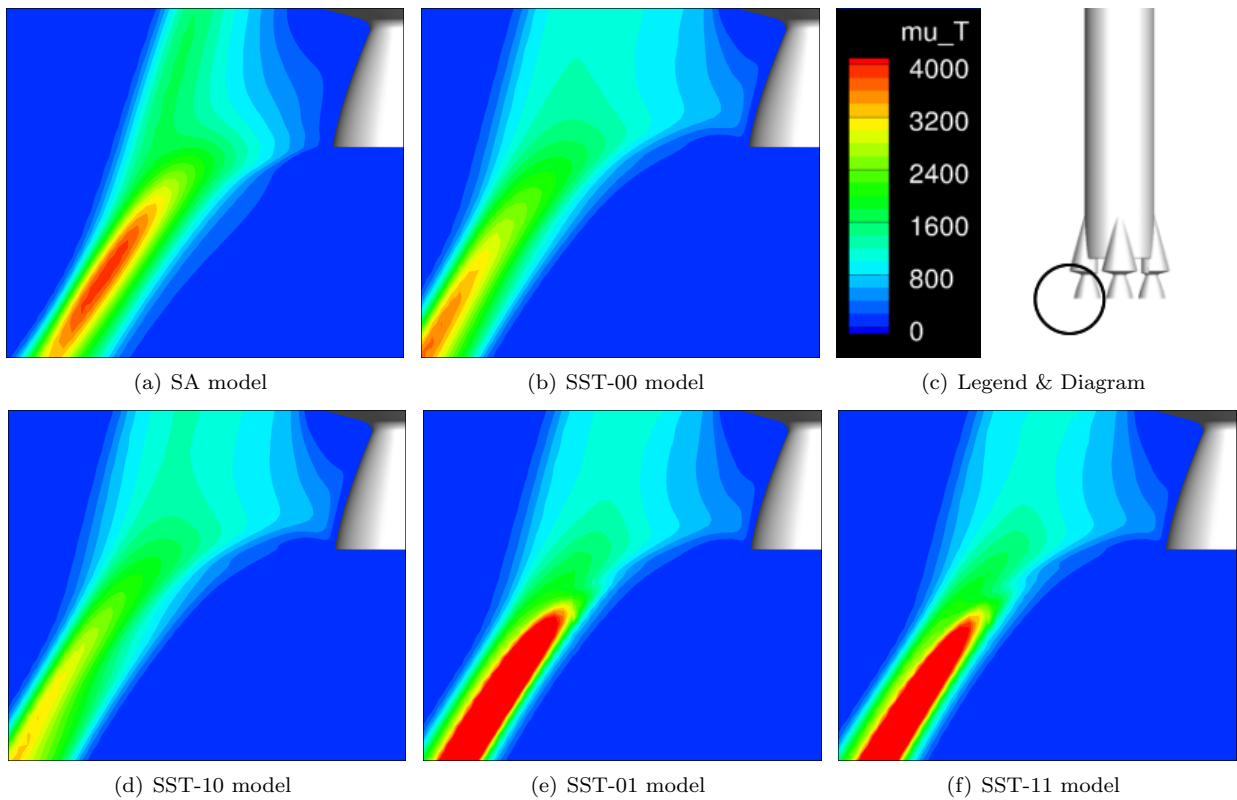


Figure 15. Contours of turbulent eddy viscosity on a slice through an outer F-1 nozzle.

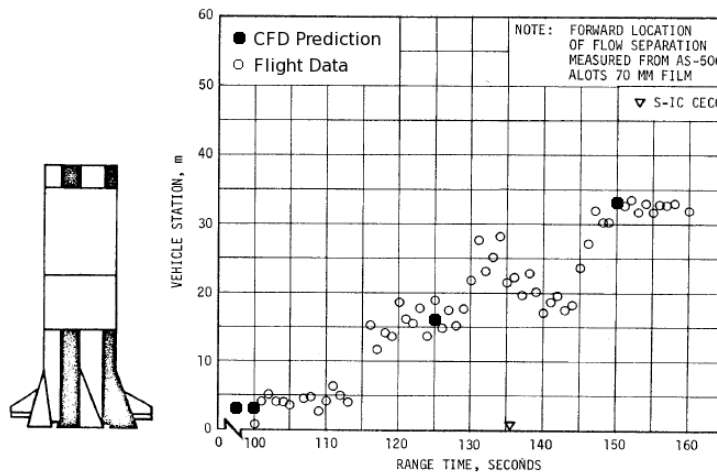


Figure 16. PIFS distances from flight data¹⁰ and CFD simulations with SST-00 turbulence model.

comparisons with the calorically perfect multi-species results were achieved. By matching these conditions, thrust and mass flow rate are consistent between single and multi-species simulations. Additional studies revealed a high PIFS distance sensitivity to the choice of turbulence model, with the best comparisons to flight data achieved with multi-species simulations using the SST model without any correction terms.

VII. Acknowledgments

The authors acknowledge the support of MSFC in providing CAD geometry, trajectory and engine data, and funding for this work. Thanks to Dr. William Chan and Daniel Schauerhamer for contributions to the overset grid system. Computations were performed on NASA Advanced Supercomputing (NAS) platforms at Ames Research Center. Portions of this work were performed under NASA contract NNA06BC19C to ELORET Corp.

References

- ¹Kiris, C., Housman, J., Gusman, M., Schauerhamer, D., Deere, K., Elmiligui, A., Abdol-Hamid, K., Parlette, E., Andrews, M., and Blevins, J., "Best Practices for Aero-Database CFD Simulations of Ares V Ascent," *AIAA*, January 2011, Accepted.
- ²Deere, K., Elmiligui, A., and Abdol-Hamid, K., "USM3D Simulations of Saturn V Plume Induced Flow Separation," *49th AIAA Aerospace Sciences Meeting, Orlando, Florida*, Jan 4-7 2011, Accepted.
- ³Springer, A., "Experimental Investigation of Plume-Induced Flow Separation on the National Launch System 1 1/2-Stage Launch Vehicle," *32nd AIAA Aerospace Sciences Meeting & Exhibit, Reno, NV*, January 10-13 1994, AIAA-1994-0030.
- ⁴CD-Adapco, "STAR-CCM+ Version 4.02.011 User Guide," 2008.
- ⁵Nichols, R. and Buning, P., "User's Manual for OVERFLOW 2.1," Version 2.1t.
- ⁶Gomez, R. and Ma, E., "Validation of a Large Scale Chimera Grid System for the Space Shuttle Launch Vehicle," *12th AIAA Applied Aerodynamics Conference, Colorado Springs, CO*, June 20-22 1994, AIAA-1994-1859.
- ⁷Chan, W., Gomez, R., Rogers, S., and Buning, P., "Best Practices in Overset Grid Generation," *32nd AIAA Fluid Dynamics Conference and Exhibit, St. Louis, Missouri*, Jun 24-26 2002, AIAA-2002-3191.
- ⁸McMillin, S. and Frink, N., "Assessment of Data Issues from LAV 19-AA Wind Tunnel Test Using TetrUSS," Task CAP-AR-41, EG-CAP-07-85, July 2007.
- ⁹Pao, S., Vatsa, V., Abdol-Hamid, K., Pirzadeh, S., J.A., S., Klopfer, G., and Taft, J.R. and Parlette, E., "Best Practice for Ascent Aero Analysis for the Ares I Configurations," *JANNAF-55*, 2008.
- ¹⁰Group, S. F. E. W., "Saturn V Launch Vehicle Flight Evaluation Report-AS-506 Apollo 11 Mission," NASA Technical Memorandum TMX-62558, NASA/MSFC, 1969.
- ¹¹Pandya, S., Chan, W., and Kless, J., "Automation of Structured Overset Mesh Generation for Rocket Geometries," *19th AIAA Computational Fluid Dynamics Conference, San Antonio, Texas*, Jun 22-25 2009, AIAA-2009-3993.
- ¹²Roe, P., "Approximate Riemann Solvers, Parameter Vectors, and Difference Schemes," *J. Computational Physics*, Vol. 43, 1981, pp. 357-372.
- ¹³Hall, L., Applebaum, M., and Eppard, M., "Saturn V Chemistry Models," October 2009, Email communication and presentation to Ames researchers.
- ¹⁴Spalart, S. and Allmaras, S., "A One-Equation Turbulence Model for Aerodynamic Flows," *30th Aerospace Sciences Meeting and Exhibit, Reno, NV*, January 1992, AIAA 92-0439.
- ¹⁵Menter, F., "Zonal Two Equation k- ω Turbulence Models For Aerodynamic Flows," *23rd Fluid Dynamics, Plasmadynamics, and Lasers Conference, Orlando, FL*, July 1993, AIAA 93-2906.
- ¹⁶Smith, B., September 29 2009, Email communication to K. S. Abdol-Hamid.
- ¹⁷Nichols, R. H., "Turbulence Models and Their Application to Complex Flows," Revision 3.0.
- ¹⁸Abdol-Hamid, K. and Pao, S. P., "Temperature Corrected Turbulence Model for High Temperature Jet Flow," *21st Applied Aerodynamics Conference, Orlando, Florida*, June 23-26 2003, AIAA 2003-4070.